Computation and characterization of local sub-filter-scale energy transfers in atmospheric flows

Davide Faranda, Valerio Lembo, Manasa Iyer, Denis Kuzzay, Sergio Chibbaro,
Francois Daviaud, Berengere Dubrulle

To cite this version:

Davide Faranda, Valerio Lembo, Manasa Iyer, Denis Kuzzay, Sergio Chibbaro, et al.. Computation and characterization of local sub-filter-scale energy transfers in atmospheric flows. Journal of the Atmospheric Sciences, 2018, 10.1175/JAS-D-17-0114.1 . hal-01566028v3

HAL Id: hal-01566028
https://hal.science/hal-01566028v3

Submitted on 15 Mar 2018

Computation and characterization of local sub-filter-scale energy transfers in atmospheric flows

Davide Faranda[1,2], Valerio Lembo [3], Manasa Iyer[4], Denis Kuzzay[5],
Sergio Chibbaro [4], Francois Daviaud[6] & Berengere Dubrulle[6]

[1] *Laboratoire des Sciences du Climat et de l'Environnement, LSCE/IPSL, CEA-CNRS-UVSQ, Université Paris-Saclay, F-91191 Gif-sur-Yvette, France*

[2] *London Mathematical Laboratory, 14 Buckingham Street, London, WC2N 6DF, UK*

davide.faranda@lsce.ipsl.fr

[3] *Meteorological Institute, University of Hamburg, Grindelberg 5, 20146 Hamburg, Germany*

[4] *Sorbonne Université, UPMC Univ Paris 06, CNRS UMR 7190, Institut Jean le Rond d'Alembert, Paris, France*

[5] *Univ Lyon, Ens de Lyon, Univ Claude Bernard, CNRS, Laboratoire de Physique, F-69342 Lyon, France*

[6] *SPEC, CEA, CNRS, Université Paris-Saclay, CEA Saclay 91191 Gif sur Yvette cedex, France*

---

*

Generated using v4.3.2 of the AMS LaTeX template

ABSTRACT

Atmospheric motions are governed by turbulent motions associated to non-trivial energy transfers at small scales (direct cascade) and/or at large scales (inverse cascade). Although it is known that the two cascades coexist, energy fluxes have been previously investigated from the spectral point of view but not on their instantaneous spatial and local structure. Here, we compute local and instantaneous sub-filter scale energy transfers in two sets of reanalyses (NCEP-NCAR and ERA-Interim) in the troposphere and the lower stratosphere for the year 2005. The fluxes are mostly positive (towards subgrid scales) in the troposphere and negative in the stratosphere reflecting the baroclinic and barotropic nature of the motions respectively. The most intense positive energy fluxes are found in the troposphere and are associated with baroclinic eddies or tropical cyclones. The computation of such fluxes can be used to characterize the amount of energy lost or missing at the smallest scales in climate and weather models.

1. Introduction

In the classical turbulence phenomenology, valid in homogeneous flows, energy is injected at large scales, transferred downscale at a constant averaged rate ε (Kolmogorov (1941) cascade) and dissipated at small scales by viscous effects (Frisch 1995). This phenomenology is based on the so-called Karman-Howarth-Monin (KHM equation), derived directly from the Navier-Stokes equation, that reads:

$$\frac{1}{2}\partial_t E + \varepsilon = -\frac{1}{4}\vec{\nabla}_\ell \cdot \langle \delta\vec{u}(\delta u)^2 \rangle + \nu \nabla_\ell^2 E, \tag{1}$$

where u is the velocity field, ν the molecular viscosity, $\langle\rangle$ means statistical average, ε is the mean non-dimensional energy injection rate, $\delta\vec{u} = \vec{u}(\vec{x}+\vec{\ell}) - \vec{u}(\vec{x})$ is the velocity increments over a distance ℓ and $E(\ell) = \langle(\delta u)^2\rangle/2$ is a measure of the kinetic energy at scale ℓ. KHM equation can be seen as the counter-part in the physical space of traditional spectral energy budgets. In stationary situations, $\frac{1}{2}\partial_t E = 0$, and the KHM equation describes how the injected energy ε is split, at each given scale, into the two terms of the r.h.s: the "inertial term", $-\frac{1}{4}\vec{\nabla}_\ell \cdot \langle \delta\vec{u}(\delta u)^2 \rangle$, that comes from the non-linear interactions, and the viscous term $\nu\nabla_\ell^2 E$, that comes from the viscosity. This energy budget is valid at any scale, and depending on the value of the scale considered, either the inertial or the viscous term dominates: for scales larger than the Kolmogorov scale $\eta = (\nu^3/\varepsilon)$, the inertial terms dominates, while the viscous term dominates for scales smaller than η. Overall, the picture is that of an energy cascade: as the scale is decreased, the energy injected at large scale ε, is gradually transferred at a constant rate to the scales $\ell < \eta$, where it is dissipated into heat. The term $-\frac{1}{4}\vec{\nabla}_\ell \cdot \langle \delta\vec{u}(\delta u)^2 \rangle$ therefore describes an energy flux at the scale ℓ, characterizing the cascade. It must be positive in order to describe a forward energy cascade, from large to small scale. This condition actually depends very much on the type of turbulence we are considering: for example in 3D turbulence, the energy cascade is forward, while in 2D incompressible turbulence, it is backward, with formation of larger and larger structures. In any case, based on this equation, the observation of the existence of a constant energy flux and on a hypothesis of self-similarity, Kolmogorov was able to find out that the energy spectrum obeys a $k^{-5/3}$ law, corresponding to a forward energy cascade.

In the atmosphere, turbulence is much more complex than the homogeneous and isotropic one because of the influence of density stratification and rotation (Holton and Hakim 2012). Turbulence in such condition is known to develop a complex dynamics, with power law energy spectra, as revealed by accurate numerical simulations and laboratory experiments (Levich and Tzvetkov 1985; Schertzer et al. 1997; Falkovich 1992; Pouquet and Marino 2013). Depending on the scale of the flow, energy transfers can be directed either towards smaller scales (direct cascade) or towards larger scales (inverse cascade) (Bartello 1995). To date, there is in fact no general consensus about the direction of cascades in the atmosphere. Observed energy spectra in the troposphere and in the lower stratosphere (Nastrom and Gage 1985) exhibit $k^{-5/3}$ law, generally connected to direct cascades, and/or k^{-3} power laws, associated to an inverse energy cascade.The inverse cascade has been historically associated to the quasi-geostrophic two dimensional dynamics induced by rotation (Charney 1971), and fed by baroclinic instability. Tung and Orlando (2003) simulated the Nastrom-Gage energy spectrum of atmospheric turbulence as a function of wavelength with a two-level quasi-geostrophic model, and were able to obtain both spectral behaviours with this simple dynamics. Kitamura and Matsuda (2006) analysed the role of stratification and rotation in the generation of the cascades, observing that in experiments without planetary rotation, the obtained spectral slope was steeper and energy transfer to larger vertical wave-numbers was increased. Some theories for a mesoscale inverse cascade for stratified (not quasi-geostrophic) turbulence were proposed by Gage (1979) and Lilly (1983) but these are no longer considered viable. According to Lindborg (2005), atmospheric mesoscale $-5/3$

energy spectra can be explained by the existence of a direct cascade arising in the limit of strong stratification while the role of planetary rotation is to inhibit the cascade process at large scales leading to an accumulation of kinetic energy and steepening of the kinetic energy spectrum at small wave numbers. Evidence of the existence of a direct energy cascade comes from high resolution direct numerical simulations of stratified flows (Lindborg 2006). They also suggest that the direction of the cascade may be crucially dependent on the ratio of the Brunt-Väisälä frequency to the rotation frequency.

A way to clarify the situation is to compute directly the energy fluxes. In the classical picture of turbulence, such energy transfers are related directly to the skewness of velocity increments $\langle \delta \mathbf{u} (\delta u)^2 \rangle$, and the direction of the cascade is provided by the sign of this quantity (negative for direct cascade, positive for inverse cascade). This quantity which is global, since it relies on space-average, has thus been used in the past to quantify the direction of the energy transfer. From the observed stratospheric third-order structure function, Lindborg and Cho (2001) argued that there is a forward energy cascade in the mesoscale range of atmospheric motions. In that study the authors pointed out that for scales smaller than 100 km the statistical inhomogeneities can be neglected while this assumption is not valid for larger scales.

Another approach relies on the spectral kinetic energy budgets (see e.g. Augier and Lindborg (2013) and Peng et al. (2015)). Alternatively, one may compute energy budget in the physical space, by considering appropriate generalization of the Karman-Howarth-Monin equation to include the influence of rotation and stratification. To this aim, Augier et al. (2012) recently considered a set of primitive equations for incompressible, non-diffusive and inviscid stably stratified fluid in the Boussinesq approximation, in order to account for both the kinetic energy (KE) and available potential energy (APE) in a modified version of the KHM equation. The primitive equations for the rotating stratified Boussinesq fluid were written as:

$$\begin{aligned} \vec{\nabla}\cdot\vec{u} &= 0, \\ \partial_t\vec{u}+\left(\vec{u}\cdot\vec{\nabla}\right)\vec{u}+2\vec{\Omega}\times\vec{u} &= -\vec{\nabla}p+b\vec{e}_z+\nu\Delta\vec{u}, \\ \partial_t b+\left(\vec{u}\cdot\vec{\nabla}\right)b &= -N^2u_z+\kappa\Delta b, \end{aligned} \tag{2}$$

where u is the velocity field,, u_z its vertical component, Ω the rotation rate, p the rescaled pressure, ν and κ the viscosity and diffusivity, $N=\sqrt{-(g/\rho_0)(d\bar{\rho}/dz)}$ the constant Brunt-Väisälä frequency, $\mathbf{e_z}$ the vertical unit vector, and $b=-\rho' g/\rho_0$ the buoyancy perturbation, g the acceleration due to gravity, ρ_0 a reference density, $\bar{\rho}(z)$ the mean profile and ρ' a density perturbation. The resulting generalized KHM equation was written as:

$$\begin{aligned} \frac{1}{2}\partial_t E+\varepsilon &= -\frac{1}{4}\vec{\nabla}_\ell\cdot\langle\delta\vec{u}\left[(\delta u)^2+\frac{(\delta b)^2}{N^2}\right]\rangle, \\ &\equiv \vec{\nabla}\cdot\vec{J}, \end{aligned} \tag{3}$$

where E is now

$$E=\frac{1}{2}\langle(\delta u)^2\rangle+\langle((\delta b)^2/N^2\rangle, \tag{4}$$

and we have omitted contributions due to viscosity and diffusivity. Note that the rotation does not enter explicitly into this energy budget because the Coriolis force is perpendicular to the flow. It enters implicitly into the energy budget through third-order correlations, that can be shown to depend explicitly on the rotation rate (Campagne 2015). This shows that the energy flux $\vec{J}$ is made of a KE flux and an APE flux, and formalizes the Lorenz Energy Cycle (LEC) description of the atmospheric energy budget (Lorenz 1955) via the conversion of APE into KE and then into dissipative heating. The KE and APE fluxes can have different direction, so that the resulting energy flux can be positive, or negative, depending on the scale, isotropy or stratification, and the corresponding direction of the energy cascade is hard to be predicted (Lovejoy and Schertzer 2010). These approaches nevertheless only provide a global in space estimate of the energy transfers, so that one cannot connect them with observed coherent structures observed in the atmosphere. One improvement of our understanding of energy transfers would therefore require their local in space and time estimates, at any given scale.

This is now possible through an important breakthrough made by Duchon and Robert (2000), who reformulated the energy budget of the Navier-Stokes equations into a form allowing for the definition of energy transfers local in space and time and valid for any geometry including when strong inhomogeneity and anisotropy are present. Its ability to provide interesting information about energy transfers at a given scale ℓ has been so far exploited in the experimental set-up of the Von Karman swirling flow to measure the scale to scale energy transfers and non viscous energy disipation (Kuzzay et al. 2015; Saw et al. 2016). The Duchon and Robert indicator requires only the 3D velocity fields and provides, for each instant, 3D maps of the sub-filter energy transfers at a scale ℓ. The interest of this formulation is that it is devoid of any adjustable parameters unlike, for exemple, local estimates of energy budgets based on LES methods (Kuzzay et al. 2015).
In this work we adapt the definition of such an indicator to the atmospheric dynamics providing the first local maps of sub-filter-scale energy transfers without any adjustable parameter. The goal of this work is i) to identify and characterize the atmospheric motions responsible for large energy transfers and ii) to compute global time and spatial average and assess whether the reanalyses over(under)-represent energy fluxes. The paper is structured as follows. After presenting the indicator, we will study these transfers in the NCEP-NCAR and ERA-Interim reanalyses - to study the sensitivity of the results to the resolution - for the year 2005. This year is ideal as it does not correspond to major ENSO events or volcanic eruptions. We investigate: i) the vertical and

horizontal global averages, ii) the distribution of energy transfers at different scales. Results are displayed in arbitrary units but in the same scale for NCEP-NCAR and ERA-Interim reanalyses. We finally discuss the implications of our results on a theoretical and practical level.

2. Methods

For any solutions of the Navier-Stokes equations, Duchon and Robert (2000) defined energy transfers in a fluid at an arbitrary scale ℓ using a local energy balance equation

$$\partial_t E^\ell + \partial_j \left(u_j E^\ell + \frac{1}{2} \left(u_j \hat{p} + \hat{u}_j p \right) + \frac{1}{4} \left(\widehat{u^2 u_j} - \widehat{u^2} u_j \right) - \nu \partial_j E^\ell \right) = -\nu \partial_j u_i \partial_j \hat{u}_i - \mathscr{D}_\ell, \qquad (5)$$

where u_i are the components of the velocity field and p the pressure, $\hat{u}$ and $\hat{p}$ their coarse-grained component at scale ℓ, $E^\ell = \frac{\hat{u}_i u_i}{2}$ is the kinetic energy per unit mass at scale ℓ (such that $\lim_{\ell \to 0} E^\ell = u^2/2$), $\mathscr{D}_\ell$ is expressed in terms of velocity increments $\delta \vec{u}(\vec{r}, \vec{x}) \overset{def}{=} \vec{u}(\vec{x} + \vec{r}) - \vec{u}(\vec{x}) \equiv \delta \vec{u}(\vec{r})$ (the dependence on ℓ and $\vec{x}$ is kept implicit) as:

$$\mathscr{D}_\ell(\vec{u}) = \frac{1}{4\ell} \int_{\mathscr{V}} d\vec{r} \, (\vec{\nabla} G_\ell)(\vec{r}) \cdot \delta \vec{u}(\vec{r}) \, |\delta \vec{u}(\vec{r})|^2, \qquad (6)$$

where G is a smooth filtering function, non-negative, spatially localized and such that $\int d\vec{r} \, G(\vec{r}) = 1$, and $\int d\vec{r} \, |\vec{r}|^2 G(\vec{r}) \approx 1$. The function G_ℓ is rescaled with ℓ as $G_\ell(\vec{r}) = \ell^{-3} G(\vec{r}/\ell)$. The choice of G slightly determines the local energy budget, in the sense that different choices of G may result in different level of kinetic or potential energy at a given scale ℓ, as well as a different repartition of injected energy between the kinetic and potential part. In that respect, the local energy budget is G-sensitive and one should choose the filter that is more appropriate to boundary conditions, and symmetry of the equations. However, we have checked on numerical simulations of incompressible Navier-Stokes equation that the spatial average of the different terms is not sensitive to the choice of G. Moreover, as shown in Duchon and Robert (2000), the choice of G has no impact on the value of $\mathscr{D}_\ell$, in the limit $\ell \to 0$, as long as it satisfies the properties specified previously. So we expect the G-sensitivity of the analysis to decrease with scale.

In the sequel, we choose a spherically symmetric function of x which has a Gaussian shape, because this filter function occurs naturally in any observational or experimental flow measurement, or in LES simulations. The corresponding energy budget will then have a straightforward physical meaning. This filter given by:

$$G_\ell(r) = \frac{1}{N}\exp(-1/(1-(r/(2\ell)^2)), \tag{7}$$

where N is a normalization constant such that $\int d^3 r G_\ell(r) = 1$. As we show later, results with this filter for two different data reanalysis are consistent, at different resolutions. This makes us confident that our results are robust.

As noticed by Duchon and Robert, the average of $\mathscr{D}_\ell(\vec{u})$ can be viewed as a weak form of the transfer term $-\frac{1}{4}\vec{\nabla}_\ell \cdot \langle \delta\vec{u}(\delta u)^2 \rangle$ in the anisotropic version of the KHM equation Eq. (1), the divergence being taken not on the term itself, but instead on the test function G_ℓ. Therefore, $\mathscr{D}_\ell(\vec{u})$ is a local version (no average is taken) of the energy transfer term of the KHM equation By construction, $\mathscr{D}_\ell(\vec{u})$ represents the amount of energy transferred at the scale ℓ by the inertial term. For scales larger than the Kolmogorov scale (which is very small in atmospheric flow), this term provides most of the energy transfer, since the viscous contribution is negligible. Its sign provides the direction of the fluxes in the scale space: a positive sign implies transfer towards the scales smaller than ℓ.

By construction, the intrinsic weak formulation of $\mathscr{D}_\ell(\vec{u})$ makes it less sensitive to noise than classical gradients, or even than the usual KHM relation: indeed, the derivative in scale is not applied directly to the velocity increments, but rather on the smoothing function, followed by a local angle averaging. This guarantees that no additional noise is introduced by the procedure.

Even more, the noise coming from the estimate of the velocity is naturally averaged out by the angle smoothing as shown in Kuzzay et al. (2015). In the same study, the authors argued that the Duchon and Robert approach was a better alternative to the widespread large eddies simulation based method for the computation of energy fluxes, since it relies on very few arbitrary hypotheses. Experimentally, in the von Karman set-up, the DR formula provided a better estimate of the energy dissipation than a LES method: in particular, estimates of the injected and dissipated powers were within 20% of the measured value using the LES-PIV method, whereas reached 98% of the actual dissipation rate of energy with the DR formula (Kuzzay et al. 2015).

This approach for atmospheric dynamics requires taking into account density stratification, and considering Boussinesq equations instead of Navier-Stokes equations. We have adapted the Duchon-Robert formalism to the Boussinesq equations. The equation for the kinetic energy is simply restated as

$$\partial_t E^\ell + \vec{\nabla}\cdot\vec{J}_K^\ell = -\nu\partial_j u_i \partial_j \hat{u}_i - \mathscr{D}_\ell + \frac{1}{2}\left(b\hat{u}_z + \hat{b}u_z\right). \tag{8}$$

Using the point-split buoyancy perturbation as fundamental variable, we can then obtain an equation related to the local variance of the buoyancy perturbation (details are given in the appendix)

$$\partial_t E_T^\ell + \vec{\nabla}\cdot\vec{J}_T^\ell = -\mathscr{D}_\ell^T - \frac{1}{2}\left(b\hat{u}_z + \hat{b}u_z\right) - \kappa\partial_j\hat{b}\partial_j b/N^2\ , \tag{9}$$

where $E_T^\ell = \frac{\hat{b}b}{2N^2}$ is the available potential energy at scale ℓ, $\mathscr{D}_\ell^T$ is expressed in terms of the increments $\delta b(\vec{r},\vec{x}) \overset{def}{=} b(\vec{x}+\vec{r}) - b(\vec{x}) \equiv \delta b(\vec{r})$ (the dependence on ℓ and $\vec{x}$ is kept implicit in the equations) as

$$\mathscr{D}_\ell^T = \frac{1}{4\ell}\int_{\mathscr{V}} d\vec{r}\ (\vec{\nabla}G_\ell)(\vec{r})\cdot\delta\vec{u}(\vec{r})\ |(\delta b)|^2/N^2. \tag{10}$$

Considering now that the energy for stratified flows is given by expression (4), we can sum equation (8) and (9), to get the total local energy balance

$$\partial_t E^\ell + \vec{\nabla}\cdot\vec{J}^\ell = -\mathscr{D}_\ell(\vec{u},b) - \nu\partial_j\hat{u}_i\partial_j u_i - \kappa\partial_j\hat{b}\partial_j b/N^2, \tag{11}$$

where

$$\vec{J}^{\ell} = \vec{J}^{\ell}_{K} + \vec{J}^{\ell}_{T}, \tag{12}$$

is the spatial energy flux, and

$$\mathscr{D}_{\ell}(\vec{u},b) = \frac{1}{4\ell}\int_{\mathscr{V}} d\vec{r}\,(\vec{\nabla}G_{\ell})(\vec{r})\cdot\delta\vec{u}\left[(\delta u)^2 + \frac{(\delta b)^2}{N^2}\right], \tag{13}$$

is the total local scale to scale energy flux. It is easy to see that the average of $\mathscr{D}_{\ell}(\vec{u},b)$ is a weak formulation of the energy transfer terms of the generalized KHM equation of Augier et al Eq. (3). The DR indicator $\mathscr{D}_{\ell}(\vec{u},b)$ is thus a local energy transfer term, that can be split into a kinetic (dynamical) part $\mathscr{D}_{\ell}(\vec{u})$ (the original DR indicator) and a potential (thermodynamic) part (the remaining part, implying the field b). In order to easily implement the expression of $\mathscr{D}_{\ell}(\vec{u},b)$ in climate models, the buoyancy parameter has been rewritten as a function of temperature T using the equation of state for dry air: $\delta b = -\delta p/\rho_0 R \cdot 1/\delta T$, where ρ_0 is a reference density at surface pressure and δp is a pressure horizontal perturbation, which is set to be about 1 hPa each 100 km. Furthermore, in Eq. 13, we set a constant Brunt-Väisälä frequency, amounting to $1.2\times10^{-2}\ s^{-1}$ (Holton and Hakim 2012). In this way, the computation of $\mathscr{D}_{\ell}(\vec{u},b)$ only requires the numerical 3D velocity u and T fields.

The sign and geometry of the zones associated with high and low values of $\mathscr{D}_{\ell}(\vec{u},b)$ will then provide interesting information about the dynamics of the energy exchange in the atmosphere. For example, a study of the occurrence of high and low values of $\mathscr{D}_{\ell}(\vec{u})$ in the von Kármán swirling flow has revealed that such events are associated with well defined, characteristic geometry of the velocity field (Saw et al. 2016). For the kinetic (dynamical) part, positive values of $\mathscr{D}_{\ell}(\vec{u})$ are measured whenever there is a strong convergence of the flow. Divergent flows are instead associated to negative values of $\mathscr{D}_{\ell}(\vec{u})$, and they point to injection of energy from the sub-filter scales. This simple description is not valid anymore when we also consider the potential (thermodynamic) component. For all these reasons, we cannot reduce the computation of $\mathscr{D}_\ell(\vec{u})$ to only that of the divergence/vorticity.

3. Analysis

For this study, outputs of the ERA-Interim and NCEP-NCAR Reanalysis 1 have been used. ERA-Interim is a modern generation reanalysis with a much higher resolution model. NCEP-NCAR was pioneering when it was developed, but is run at a comparatively low resolution and does not take advantage of as many observations.

ERA-Interim is the currently operational Reanalysis product at the European Center for Medium-Range Weather Forecasting (ECMWF) (Dee et al. 2011). Released in 2007, it provides reanalyzed data from 1979 to nowadays, stored at an original T255 spectral resolution (about 80 km horizontal resolution), with 60 vertical hybrid model levels. A 12h four-dimensional variational data assimilation (4D-Var) is adopted. As a forecast model, the Integrated Forecast Model (IFS), Cy31r2 release, is used, fully coupling modules for the atmosphere, ocean waves and land surface. Sea-surface temperatures (SST) and sea-ice concentration (SIC) are ingested as boundary conditions and interpolated on a reduced-Gaussian grid as needed. In our case zonal, meridional and vertical wind components are considered at a $0.75^\circ \times 0.75^\circ$ horizontal resolution over 12 pressure levels between 1000 and 100 hPa. A 12h time-step is considered. Known problems concerning these datasets are the lack of dry mass conservation (Berrisford et al. 2011) and the slight asymmetry between evaporation and precipitation (Dee et al. 2011). The turbulent fluxes are based on the tiled ECMWF scheme for surface exchanges over land (Viterbo and Beljaars 1995; Viterbo and Betts 1999). Each gridbox is divided into up to six fractions (over land) depending on the type of surface, having different transfer coefficients based on a

Monin-Obukhov formulation. Similarly, over oceans, two different coefficients are used for stable and unstable conditions (Beljaars 1995).

NCEP-NCAR Reanalysis 1 has been developed in a joint effort by the National Center for Environmental Prediction (NCEP) and the National Center for Atmospheric Research (NCAR) (Kalnay et al. 1996). The simulation is operational since January 1995, covering a period from 1948 to nowadays. Data assimilation is performed via a 3D variational scheme (Parrish and Derber 1992). It features a T62 spectral resolution, corresponding to a $2.5^\circ \times 2.5^\circ$ horizontal grid (about 200 km horizontal resolution), with 28 sigma levels. Most of the major physical processes involving the climate system are parametrized. SST, SIC, snow cover, albedo, soil wetness and roughness length are ingested as boundary conditions. Data are archived at an original 6h time-step, and such a temporal resolution is retained for our analysis. The atmospheric model which provides the NCEP/NCAR reanalysis data, uses bulk aerodynamic formulas to estimate the turbulent fluxes, with exchange coefficients depending on empirical profiles extending the Monin-Obukhov similarity relationship (Miyakoda and Sirutis 1986). For more details on the comparison between different subgrid parametrization of surface fluxes, one might refer to Brunke et al. (2011).

a. Analysis of local energy transfers

1) YEAR AND SEASONS' AVERAGES OF LOCAL ENERGY TRANSFERS

We begin the analysis by studying the latitudinal averages and the spatial features of the DR indicator for both the ERA-Interim reanalysis and the coarser NCEP-NCAR reanalysis. To enable comparison between the two datasets, one has to choose the analysis length larger than the resolution scale of NCEP-NCAR (200km) since going below the resolution size introduces spurious effects dependent on the filter design. On the other hand, since we want to have as much details as possible, we have to choose the smallest scale consistent with those requirements. Here, we thus adopt a scale of $\ell = 220$ km, this scale being the smallest that provide reliable estimates of DR indicator. A further discussion of the dependence of the results with scale is done in section 3.a.3.

Results obtained for both reanalysis are consistent with each other, as can be checked from Figure 1 (ERA) and Fig. 2 (NCEP). The gross features do not depend on whether one undertakes a year average (a,d), or seasonal (b,c,e,f): in the panels (a,b,c), which show height dependence of the longitudinally averaged $\langle \mathscr{D}_\ell(\vec{u},b)\rangle_{long}$, one observes the the total local energy transfers $\mathscr{D}_\ell(\vec{u},b)$ are mostly positive in the troposphere, about zero at the tropopause and negative in the lower stratosphere. By looking at cuts at different pressure levels, one can look more precisely about the spatial distribution of the yearly and seasonal averages of $\langle \mathscr{D}_\ell(\vec{u},b)\rangle_{time}$. Close to the ground ($P = 1000$ hPa), the DR indicator is approximately zero except in proximity of sharp elevation gradients (Antarctica costs, Himalaya, Greenland and Andes mountain ranges). By splitting the local energy transfers is their kinetic $\langle \mathscr{D}_\ell(\vec{u})\rangle_{time}$ and thermodynamic part $\langle \mathscr{D}_\ell^T\rangle_{time}$ (Fig. S1-S4 of Supplementary Material), one sees that this effect is mostly due to the the density fluctuations (i.e. the thermodynamic component of the DR indicator) that produce these negative fluxes.

In the middle troposphere ($P = 500$ hPa), the behavior of $\mathscr{D}_\ell(\vec{u},b)$ is associated to that of the jet stream, since the most intense positive patterns are observed in winter for the northern hemisphere and summer for the southern hemisphere. In the lower stratosphere ($P = 100$ hPa), $\mathscr{D}_\ell(\vec{u},b)$ is negative at the middle latitudes, and become slightly positive in polar regions and in the intertropical convergence zone. Overall, the splitting between the kinetic and thermodynamic component detailed in the Supplementary material suggests that the dynamical component dominates with respect to the thermodynamic one, although the DR thermodynamic contributions are significant especially in the proximity of the ground.

2) CORRELATION WITH ENERGY SPECTRUM

The above result shows that the kinetic energy flux are globally positive in the troposphere, indicating a *direct* kinetic energy cascade, while they are negative in the lower stratosphere indicating a *inverse* kinetic energy cascade. Our results are therefore consistent with those found by Peng et al. (2015) who also found upscale transfer in the lower stratosphere at outer mesoscale length scales and downscale transfers at scales smaller than 360 km (KE) or 200 km (APE).

To get some insight on these cascades, we have further computed the kinetic horizontal energy spectra where k is the inverse of the wavelength from the horizontal velocity fields at different pressure levels in the two reanalysis. They are reported in Figure 3. One sees that for $P \leq 500$ hPa (corresponding to the stratosphere), the energy spectrum is mostly scaling like k^{-3}, while for $P \geq 500$ hPa (middle troposphere), the energy spectrum scales like $k^{-5/3}$, at least for scales larger than $\ell = 220$ km-in agreement with the Nastrom-Gage spectrum in the lower stratosphere at scales between 10^3 and 10^2 km. In the ERA Interim data, the spectrum steepens below this scale and is closer to k^{-2}. These values are however to be taken with caution, since our resolution does not able one to distinguish clearly between a slope of $-5/3$ and $-7/5$ or $-11/5$ and -3, which are classical spectral slope that appear in rotating stratified or quasi 2D turbulence. Moreover, the spectra are computed on a Cartesian grid which weight oddly higher latitudes, so that it is hard to trust results NCEP-NCAR reanalysis below $\ell = 220$ km. The difference in spectra between the troposphere and stratosphere is a well-observed property of the kinetic energy spectra in the atmosphere, and several explanations have been proposed for that, some of them complementary to each other. The existence of an individual range spanning from planetary wavelengths to the edge of the sub-inertial range) in the troposphere has been observed, e.g. by Koshyk et al. (1999). They found that above 250 hPa there is a transition to a two-ranges spectrum at synoptic scales, so that the sub-inertial range makes his way deep until about 2000 km wavelength and the spectrum exhibits a slope of $-5/3$. At larger wavelengths the slope is still equal to -3. They explain this transition with the rotational component of the kinetic energy decaying with height at a higher rate than the divergent component. Accordingly, Burgess et al. (2013) attribute this transition to the zonal mean-eddy interaction overcoming the eddy-eddy interaction in setting up the transient kinetic energy peak. Žagar et al. (2017) propose also that this might be attributed to the predominant role of non-linear inertial-gravity waves. In accurate numerical simulations, Pouquet et al. (2017) have also shown that by changing the value of f/N, one also change the value of the crossover between the large scales involving an inverse energy cascade, and the small scale, involving a direct energy cascade. In the terrestrial atmosphere the value of f is practically constant, whereas N can vary up to a factor 2 between troposphere and stratosphere, thus changing the direction of the cascade.

3) PROBABILITY DISTRIBUTION FUNCTIONS OF INSTANTANEOUS LOCAL ENERGY TRANSFERS

In addition to time average, it is also interesting to study the probability distribution function of instantaneous local energy transfers, $\mathscr{D}_\ell(\vec{u},b)$ at a different height (pressure level), and see how it varies with scale and height. This is provided in Figure 4 for ERA-Interim and Figure 5 for NCAR reanalyses. Panels (b,d,f) show the distributions at each level for $\ell = 220$ km. Panels (a,b) show the kinetic component $\mathscr{D}_\ell(\vec{u},0)$, panels (c,d) the thermodynamic component $\mathscr{D}_\ell^T$ and (e,f) the total $\mathscr{D}_\ell(\vec{u},b)$. Tables S1 ans S2 of the supplemental material report the values of mean, standard deviation, skewness and kurtosis as a function of the height for the total DR indicator.

Overall, all distributions are skewed, and exhibit fat tails. The sign of the skewness depends on the height: for both the total and kinetic component, it is positive in the lower troposphere, and negative for $P < 500$ hPa, in agreement with the time averages. For the thermodynamic part, the behaviour is opposite, with a negative skewness at low altitude ($P > 700hPa$) and positive skewness at large altitude. In such case, the distribution is totally asymmetric, and includes only positive transfer, indicating that in the high part of the atmosphere, the density fluctuations only contribute to a downscale energy transfer. Although there is agreement between the ERA interim and the NCEP-NCAR data, the latter shows fatter tails. This might be due either to the different resolution of the datasets and/or on the different physical parametrizations.

Looking now at the dependence with scale at fixed height, we see that both the kinetic and total local energy transfer display similar behaviour, with a tendency to have fatter tails with decreasing scales. This means that the energy imbalance of the reanalysis is reduced when we look at motions whose characteristic scales are larger. This type of behaviour, also observed in local energy transfers measured in a laboratory turbulent von Karman flow (Saw et al. 2016), might be due to the fact that, at larger scales, the atmosphere becomes more wave like (and so less turbulent) (Rhines 1979). Regarding the thermodynamical part of the transfer, the scale dependence is much more mild on the positive side of the distribution, and even absent in the negative part of the distribution.

4) POSSIBLE INTERPRETATION

A possible way to explain the sign of the DR indicators is to invoke the relation between baroclinic and barotropic flows and direct and inverse cascades. In Tung and Orlando (2003), it is argued that he baroclinic motions responsible for the genesis and decay of extratropical cyclones are mostly associated to direct cascades (corresponding to positive $\mathscr{D}_\ell(\vec{u}, b)$), while the essentially barotropic motions governing the lower stratosphere dynamics (Salby (1996), Chapter 17), are associated to an inverse energy cascade (that would correspond to negative values of $\mathscr{D}_\ell(\vec{u},b)$). To check such interpretation, we have analyzed the maps of $\mathscr{D}_\ell(\vec{u})$ collected each 6 or 12h depending on the datasets. They are collected for NCEP-NCAR in the supplementary video. Large positive and negative values of the DR indicator are found as dipoles in baroclinic eddies. When increasing the scale ℓ of the analysis, the tails become lighter as the local positive and negative contributions get averaged out.

4. Discussion

Weather and climate models do not resolve the viscous scales, which for the atmospheric motions are order of 0.1 mm (Priestley 1959). Up to date, their resolution ranges from $\simeq$ 2 km of regional weather models to $\simeq$ 100 km of global climate models. To correctly represent dissipation effects at a scale ℓ, the turbulent cascade needs to be parametrized at each grid point depending on the type of motion and the geographical constraints. Despite the importance of such energy transfers, their distribution and their time and spatial behavior is known only partially through field campaigns (Lübken 1997) or by global averages (Sellers 1969; Seinfeld and Pandis 2016). This does not ensure a global coverage and does not tell the direction of the energy transfers in the free troposphere. In this paper, we have used Duchon and Robert (2000) to compute and characterize the distribution of instantaneous and local sub-filter energy transfers in the atmosphere using 3D velocity fields obtained in NCEP-NCAR and ERA-Interim reanalysis. Those energy transfers are highly correlated with the baroclinic eddies occurring at mid-latitudes and with severe tropical cyclones. Our computation of local energy transfer provides the direction of the local energy cascade at a certain scale ℓ in physical space. At the grid resolution Δx, the value of $\mathscr{D}_{\Delta x}(\vec{u},b)$ is an exact measure of the amount of energy *that must be transferred to subgrid scales* (positive DR contributions) or *that must be injected from the subgrid scales* (negative contributions) in order to equilibrate energy budgets. If the simulation is perfectly resolved, so that $\Delta x = \eta$, this equilibration is of course guaranteed by the contribution due to viscosity. In most cases, however, the Kolmogorov scale is not resolved, and one needs to artificially increase the viscosity, so as to absorb or produce this energy flux. The information about $\mathscr{D}_{\Delta x}(\vec{u}, b)$ could then be used to interactively adjust the viscosity to account for the energy conservation laws in the atmosphere (Lucarini and Ragone 2011). Furthermore, the expression of $\mathscr{D}_\ell(\vec{u})$ is separable in a dynamical and a thermodynamic contributions. Although most of the total $\mathscr{D}_\ell(\vec{u}, b)$ contribution is due to the dynamical component, negative fluxes are found at the ground in presence of mountain ranges and sharp temperature/pressure gradients, positive fluxes in the middle troposphere reinforce the dynamic contrbutions. We have also observed that extreme events as tropical and extratropical storms are associated with large values of $\mathscr{D}_\ell(\vec{u}, b)$, even at the ground.

The quantity $\mathscr{D}_\ell(\vec{u}, b)$ could also be a proxy of the flux of energy that can be exploited in wind turbines (Miller et al. 2011, 2015). Although our analysis is performed for large scale general circulation models, the Duchon and Robert (2000) formula can be applied to regional climate and weather prediction models. At smaller scales, it will be extremely interesting to analyze the relation between $\mathscr{D}_\ell(\vec{u}, b)$ and the genesis of extreme wind gusts or even tornadoes. At such scales, one could investigate the distributions of $\mathscr{D}_\ell(\vec{u}, b)$ to the instantaneous subgrid scales dissipation obtained by field measurements (Higgins et al. 2003). It will also been worth investigating whether adaptive asymptotic methods, as those proposed by Klein et al. (2001) or the Lagrangian scale-dependant models for the subgrid scales in Large Eddy Simulations (Bou-Zeid et al. 2004), afford better energy balances, i.e. the spatial and temporal average of $\mathscr{D}_\ell(\vec{u}, b)$ is closer to zero.

It is evident that the resolution plays an important role in determining spurious energy fluxes by looking at the difference in the $\mathscr{D}_\ell(\vec{u}, b)$ indicator near the ground (NCAR vs ERA-Interim reanalysis). However, it is positively surprising that the average spatial and vertical structure of the indicators is very similar in both reanalysis.

Several waves phenomena in the atmospheric - gravity and Rossby waves - are tied to these horizontal density variations, and are associated with energy conversion between available potential and kinetic energy. One key question is whether this diagnostic may incorrectly assess such energy conversion as an energy transfer across scale. For future research directions, it might be worth applying the diagnostic to a simple gravity or Rossby wave model.

APPENDIX

A1. Derivation of the local Duchon-Robert equation for Boussinesq equations

We start from the Boussinesq equation Eqs. (2) for the buoyancy perturbation and write it at two different position, $\vec{x}$ and $\vec{x}'$ for $b(\vec{x})$ and $b' = b(\vec{x}')$ and $u(\vec{x})$ and $u' = u(\vec{x}')$:

$$\partial_t b + \partial_j (u_j b) = -N^2 u_z + \kappa \partial_j^2 b, \tag{A1}$$

$$\partial_t b' + \partial_j (u'_j b') = -N^2 u'_z + \kappa \partial_j^2 b', \tag{A2}$$

Multiplying the equation (A1) by b' and equation (A2) by b and adding the results we obtain

$$\partial_t (bb') + b\partial_j (b' u'_j) + b' \partial_j (b u_j) = -N^2 \left(b' u_z + b u'_z \right) + \kappa \left(b' \partial_j^2 b + b \partial_j^2 b' \right) \ . \tag{A3}$$

To simplify the equation, we can write the diffusive term as

$$b' \partial_j^2 b + b \partial_j^2 b' = \partial_j^2 bb' - 2\partial_j b \partial_j b' \ , \tag{A4}$$

while the nonlinear can be written as

$$b \partial_j b' u'_j + b' \partial_j b u_j = b \delta u_j \partial_j b' + \partial_j b u_j b' \ , \tag{A5}$$

where $\delta u_j = u'_j - u_j$ as before. Considering the term $(u'_j - u_j)(b' - b)^2 = \delta u_j (\delta b)^2$, it reads as

$$\delta u_j (\delta b)^2 = b'^2 (\delta u_j) + b^2 (\delta u_j) - 2b' (u'_j - u_j) b \tag{A6}$$

Using now the identities $\nabla_r \cdot (\delta \mathbf{u}) = \nabla_r \cdot \mathbf{u}' = 0$, and after some manipulations we have:

$$b\delta u_j \partial_j b' = \frac{1}{2}\left[\partial_j(b'^2 \delta u_j) - \partial_j(\delta u_j (\delta b)^2)\right] + \partial_j b u_j b' \tag{A7}$$

Substituting the results from the equations (A4) and (A7) and multiplying both the sides by $1/2$ and simplifying gives:

$$\begin{aligned}\partial_t(\frac{1}{2}bb') + \frac{1}{2}\partial_j\left((u_j b')b + \frac{1}{2}b'^2\delta u_j - \kappa\partial_j(bb')\right) &= \frac{1}{4}\nabla_r \cdot \delta\vec{u}(\delta b)^2 - \kappa\partial_j b\partial_j b' \\ &\quad -\frac{N^2}{2}\left(bu'_z + b'u_z\right)\ ;\end{aligned} \tag{A8}$$

Applying the filter operator G_ℓ, and noting $\hat{f} = f * G_\ell$ ($*$ being the convolution), we get:

$$\begin{aligned}\partial_t(\frac{1}{2}b\hat{b}) &+ \vec{\nabla}\cdot\left(\frac{1}{2}(\vec{u}\hat{b})b + \frac{1}{4}\widehat{(b^2\vec{u})} - \frac{1}{4}\widehat{(b^2)}\vec{u}) - \kappa\vec{\nabla}(\frac{1}{2}b\hat{b})\right) \\ &= -\frac{1}{4\ell}\int d\vec{r}(\vec{\nabla}G)_l \cdot \delta\vec{u}(r)(\delta b)^2 - \kappa\vec{\nabla}b\cdot\vec{\nabla}\hat{b} - \frac{N^2}{2}\left(b\hat{u}_z + \hat{b}u_z\right).\end{aligned} \tag{A9}$$

Introducing $E_T^\ell = b\hat{b}/2N^2$,the available potential energy at scale ℓ , and the terms

$$\vec{J}_T^\ell = \left(\frac{1}{2}(\vec{u}\hat{b})b + \frac{1}{4}\widehat{(b^2\vec{u})} - \frac{1}{4}\widehat{(b^2)}\vec{u}) - \kappa\vec{\nabla}(\frac{1}{2}b\hat{b})\right)/N^2, \tag{A10}$$

$$\mathscr{D}_\ell^b = \frac{1}{4l}\int d^d r(\vec{\nabla}G)_l \cdot \delta\vec{u}(r)(\delta b)^2/N^2, \tag{A11}$$

we get the equation , Eq (9) of section 2.

Now, to study the inviscid limit $\nu \to 0$, we take the limit $\ell \to\ 0$ and introducing the available potential energy $E_T = b^2/2N^2$, the equation finally simplifies to:

$$\partial_t E_T + \vec{\nabla}\cdot(\frac{1}{2}\vec{u}E_T) - \kappa\nabla^2 E_T = -bu_z - \mathscr{D}^b - \kappa(\nabla b)^2/N^2, \tag{A12}$$

with

$$\mathscr{D}^b = \lim_{l\to 0}\mathscr{D}_\ell^b. \tag{A13}$$

The equation for the kinetic energy has been derived in Duchon and Robert (2000), without the term due to rotation and buoyancy. For the rotation, it is straightforward to see that it only adds a terms $\vec{u}\cdot(2\vec{\Omega}\times\hat{\vec{u}})+\hat{\vec{u}}\cdot(2\vec{\Omega}\times\vec{u})$ which vanishes, due to the symmetry of the × operator. The buyoancy adds a new term that can be simply included, so that the equation for the kinetic energy writes as:

$$\begin{aligned}\partial_t E^\ell \quad &+ \quad \partial_j\left(\hat{u}_j E^\ell+\frac{1}{2}\left(u_j\hat{p}+\hat{u}_j p\right)+\frac{1}{4}\left(\widehat{u^2u_j}-\frac{1}{4}\widehat{u^2}u_j\right)-\nu\partial_j E^\ell\right)= \\ &- \quad \nu\partial_j u_i\partial_j\hat{u}_i-\mathscr{D}_\ell+\frac{1}{2}\left(b\hat{u}_z+\hat{b}u_z\right), \qquad \text{(A14)}\end{aligned}$$

with $\mathscr{D}_\ell$ being given by Eq. 6. Introducig the KE spatial flux:

$$\vec{J}_K^\ell=\hat{\vec{u}}E^\ell+\frac{1}{2}\left(\vec{u}\hat{p}+\hat{\vec{u}}p\right)+\frac{1}{4}\left(\widehat{(u^2\vec{u})}-\frac{1}{4}\widehat{(u^2)}\vec{u}\right)-\nu\vec{\nabla}E^\ell, \qquad \text{(A15)}$$

we get Eq. (8) of section 2. The fact that the rotation doe no enter explicitly into the kinetic energy budget is well-known, and due to the fact that the Coriolis force does not produce energy. However, it influences the energy cascade through the energy redistribution by nonlinear mechanisms such as resonant wave interactions (Campagne et al. 2014). This process is taken into account in term $\mathscr{D}_\ell$ via the the third-order moment.

Acknowledgments. D. Faranda was supported by ERC grant No. 338965. DF thanks G. Messori and N. Vercauteren for useful discussions and comments on the paper.

References

Augier, P., S. Galtier, and P. Billant, 2012: Kolmogorov laws for stratified turbulence. *Journal of Fluid Mechanics*, **709**, 659–670.

Augier, P., and E. Lindborg, 2013: A new formulation of the spectral energy budget of the atmosphere, with application to two high-resolution general circulation models. *Journal of the Atmospheric Sciences*, **70 (7)**, 2293–2308.

Bartello, P., 1995: Geostrophic adjustment and inverse cascades in rotating stratified turbulence. *Journal of the atmospheric sciences*, **52 (24)**, 4410–4428.

Beljaars, A., 1995: The parametrization of surface fluxes in large-scale models under free convection. *Quarterly Journal of the Royal Meteorological Society*, **121 (522)**, 255–270.

Berrisford, P., P. Kållberg, S. Kobayashi, D. Dee, S. Uppala, a. J. Simmons, P. Poli, and H. Sato, 2011: Atmospheric conservation properties in ERA-Interim. *Quarterly Journal of the Royal Meteorological Society*, **137 (July)**, 1381–1399, doi:10.1002/qj.864.

Bou-Zeid, E., C. Meneveau, and M. B. Parlange, 2004: Large-eddy simulation of neutral atmospheric boundary layer flow over heterogeneous surfaces: Blending height and effective surface roughness. *Water Resources Research*, **40 (2)**.

Brunke, M. A., Z. Wang, X. Zeng, M. Bosilovich, and C.-L. Shie, 2011: An assessment of the uncertainties in ocean surface turbulent fluxes in 11 reanalysis, satellite-derived, and combined global datasets. *Journal of Climate*, **24 (21)**, 5469–5493.

Burgess, B. H., A. R. Erler, and T. G. Shepherd, 2013: The troposphere-to-stratosphere transition in kinetic energy spectra and nonlinear spectral fluxes as seen in ecmwf analyses. *Journal of the Atmospheric Sciences*, **70 (2)**, 669–687.

Campagne, A., 2015: Cascades dénergie et turbulence dondes dans une expérience de turbulence en rotation. Ph.D. thesis, Université Paris Sud.

Campagne, A., B. Gallet, F. Moisy, and P.-P. Cortet, 2014: Direct and inverse energy cascades in a forced rotating turbulence experiment. *Phys. Fluids*, **26 (125112)**.

Charney, J. G., 1971: Geostrophic turbulence. *Journal of the Atmospheric Sciences*, **28 (6)**, 1087–1095.

Dee, D. P., and Coauthors, 2011: The ERA-Interim reanalysis: configuration and performance of the data assimilation system. *Quarterly Journal of the Royal Meteorological Society*, **137 (656)**, 553–597, doi:10.1002/qj.828, URL http://doi.wiley.com/10.1002/qj.828.

Duchon, J., and R. Robert, 2000: Inertial energy dissipation for weak solutions of incompressible euler and navier-stokes equations. *Nonlinearity*, **13 (1)**, 249.

Falkovich, G., 1992: Inverse cascade and wave condensate in mesoscale atmospheric turbulence. *Physical review letters*, **69 (22)**, 3173.

Frisch, U., 1995: *Turbulence: the legacy of AN Kolmogorov*. Cambridge university press.

Gage, K., 1979: Evidence far ak- 5/3 law inertial range in mesoscale two-dimensional turbulence. *Journal of the Atmospheric Sciences*, **36 (10)**, 1950–1954.

Higgins, C. W., M. B. Parlange, and C. Meneveau, 2003: Alignment trends of velocity gradients and subgrid-scale fluxes in the turbulent atmospheric boundary layer. *Boundary-Layer Meteorology*, **109 (1)**, 59–83.

Holton, J. R., and G. J. Hakim, 2012: *An introduction to dynamic meteorology*, Vol. 88. Academic press.

Kalnay, E., and Coauthors, 1996: The NCEP/NCAR 40-year reanalysis project. *Bulletin of the American Meteorological Society*, **77**, 437–471, doi:10.1175/1520-0477(1996)077⟨0437:TNYRP⟩2.0.CO;2.

Kitamura, Y., and Y. Matsuda, 2006: The kh- 3 and kh- 5/3 energy spectra in stratified turbulence. *Geophysical research letters*, **33 (5)**.

Klein, R., N. Botta, T. Schneider, C.-D. Munz, S. Roller, A. Meister, L. Hoffmann, and T. Sonar, 2001: Asymptotic adaptive methods for multi-scale problems in fluid mechanics. *Practical Asymptotics*, Springer, 261–343.

Kolmogorov, A. N., 1941: Dissipation of energy in locally isotropic turbulence. *Dokl. Akad. Nauk SSSR*, Vol. 32, 16–18.

Koshyk, J. N., B. A. Boville, K. Hamilton, E. Manzini, and K. Shibata, 1999: Kinetic energy spectrum of horizontal motions in middle-atmosphere models. *Journal of Geophysical Research: Atmospheres*, **104 (D22)**, 27 177–27 190.

Kuzzay, D., D. Faranda, and B. Dubrulle, 2015: Global vs local energy dissipation: The energy cycle of the turbulent von kármán flow. *Physics of Fluids (1994-present)*, **27 (7)**, 075 105.

Levich, E., and E. Tzvetkov, 1985: Helical inverse cascade in three-dimensional turbulence as a fundamental dominant mechanism in mesoscale atmospheric phenomena. *Physics reports*, **128 (1)**, 1–37.

Lilly, D. K., 1983: Stratified turbulence and the mesoscale variability of the atmosphere. *Journal of the Atmospheric Sciences*, **40 (3)**, 749–761.

Lindborg, E., 2005: The effect of rotation on the mesoscale energy cascade in the free atmosphere. *Geophysical research letters*, **32 (1)**.

Lindborg, E., 2006: The energy cascade in a strongly stratified fluid. *Journal of Fluid Mechanics*, **550**, 207–242.

Lindborg, E., and J. Y. Cho, 2001: Horizontal velocity structure functions in the upper troposphere and lower stratosphere. ii- theoretical considerations. *Journal of geophysical research*, **106**, 10.

Lorenz, E. N., 1955: Available potential energ and the maintenance of the general. *Tellus*, **7**, 2.

Lovejoy, S., and D. Schertzer, 2010: Towards a new synthesis for atmospheric dynamics: space–time cascades. *Atmospheric Research*, **96 (1)**, 1–52.

Lübken, F.-J., 1997: Seasonal variation of turbulent energy dissipation rates at high latitudes as determined by in situ measurements of neutral density fluctuations. *Journal of Geophysical Research: Atmospheres*, **102 (D12)**, 13 441–13 456.

Lucarini, V., and F. Ragone, 2011: Energetics of climate models: Net energy balance and meridional enthalpy transport. *Reviews of Geophysics*, **49 (1)**.

Miller, L. M., N. A. Brunsell, D. B. Mechem, F. Gans, A. J. Monaghan, R. Vautard, D. W. Keith, and A. Kleidon, 2015: Two methods for estimating limits to large-scale wind power generation. *Proceedings of the National Academy of Sciences*, **112 (36)**, 11 169–11 174.

Miller, L. M., F. Gans, and A. Kleidon, 2011: Estimating maximum global land surface wind power extractability and associated climatic consequences. *Earth Syst. Dynam*, **2 (1)**, 1–12.

Miyakoda, K., and J. Sirutis, 1986: Manual of the e-physics. *Available from Geophysical Fluid Dynamics Laboratory, Princeton University, PO Box*, **308**.

Nastrom, G., and K. S. Gage, 1985: A climatology of atmospheric wavenumber spectra of wind and temperature observed by commercial aircraft. *Journal of the atmospheric sciences*, **42 (9)**, 950–960.

Parrish, D. F., and J. C. Derber, 1992: The national meteorological center's spectral statistical-interpolation analysis system. *Monthly Weather Review*, **120 (8)**, 1747–1763, doi:10.1175/1520-0493(1992)120⟨1747:TNMCSS⟩2.0.CO;2, URL http://dx.doi.org/10.1175/1520-0493(1992)120⟨1747:TNMCSS⟩2.0.CO;2.

Peng, J., L. Zhang, and J. Guan, 2015: Applications of a moist nonhydrostatic formulation of the spectral energy budget to baroclinic waves. part i: The lower-stratospheric energy spectra. *Journal of the Atmospheric Sciences*, **72 (5)**, 2090–2108.

Pouquet, A., and R. Marino, 2013: Geophysical turbulence and the duality of the energy flow across scales. *Physical review letters*, **111 (23)**, 234 501.

Pouquet, A., R. Marino, P. D. Mininni, and D. Rosenberg, 2017: Dual constant-flux energy cascades to both large scales and small scales. *Physics of Fluids*, **29 (11)**, 111 108.

Priestley, C. H. B., 1959: *Turbulent transfer in the lower atmosphere*. University of Chicago Press Chicago.

Rhines, P. B., 1979: Geostrophic turbulence. *Annual Review of Fluid Mechanics*, **11 (1)**, 401–441.

Salby, M. L., 1996: *Fundamentals of atmospheric physics*, Vol. 61. Academic press.

Saw, E.-W., D. Kuzzay, D. Faranda, A. Guittonneau, F. Daviaud, C. Wiertel-Gasquet, V. Padilla, and B. Dubrulle, 2016: Experimental characterization of extreme events of inertial dissipation in a turbulent swirling flow. *Nature Communications*, **7**, 12 466.

Schertzer, D., S. Lovejoy, F. Schmitt, Y. Chigirinskaya, and D. Marsan, 1997: Multifractal cascade dynamics and turbulent intermittency. *Fractals*, **5 (03)**, 427–471.

Seinfeld, J. H., and S. N. Pandis, 2016: *Atmospheric chemistry and physics: from air pollution to climate change*. John Wiley & Sons.

Sellers, W. D., 1969: A global climatic model based on the energy balance of the earth-atmosphere system. *Journal of Applied Meteorology*, **8 (3)**, 392–400.

Tung, K. K., and W. W. Orlando, 2003: The k- 3 and k- 5/3 energy spectrum of atmospheric turbulence: Quasigeostrophic two-level model simulation. *Journal of the atmospheric sciences*, **60 (6)**, 824–835.

Viterbo, P., and A. C. Beljaars, 1995: An improved land surface parameterization scheme in the ecmwf model and its validation. *Journal of Climate*, **8 (11)**, 2716–2748.

Viterbo, P., and A. K. Betts, 1999: Impact on ecmwf forecasts of changes to the albedo of the boreal forests in the presence of snow. *Journal of Geophysical Research: Atmospheres*, **104 (D22)**, 27 803–27 810.

Žagar, N., D. Jelić, M. Blaauw, and P. Bechtold, 2017: Energy spectra and inertia–gravity waves in global analyses. *Journal of the Atmospheric Sciences*, **74 (8)**, 2447–2466.

LIST OF FIGURES

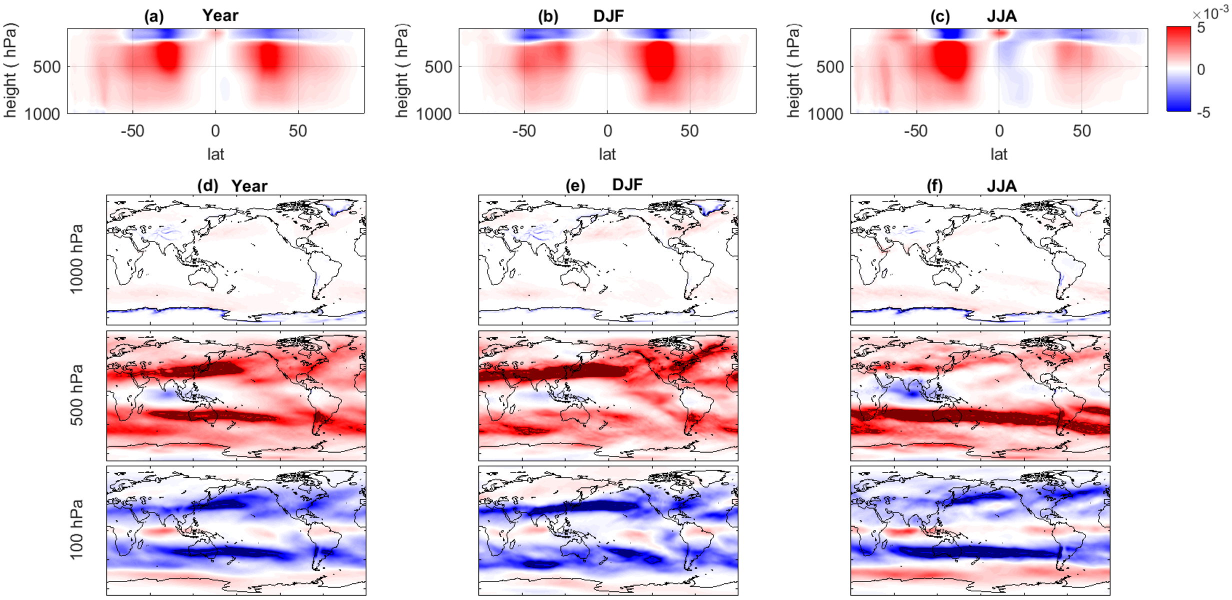

579 FIG. 1. Distribution of $\mathscr{D}_\ell(\vec{u}, b)$ for $\ell = 220$ Km and the ERA-Interim reanalysis. (a-c) longitudinal averages, 580 (d-e-f) maps at three different fixed height: 1000 hPa, 500 hPa and 100hPa. (a,d) yearly averages, (b,e) winter 581 averages, (c,f) summer averages.

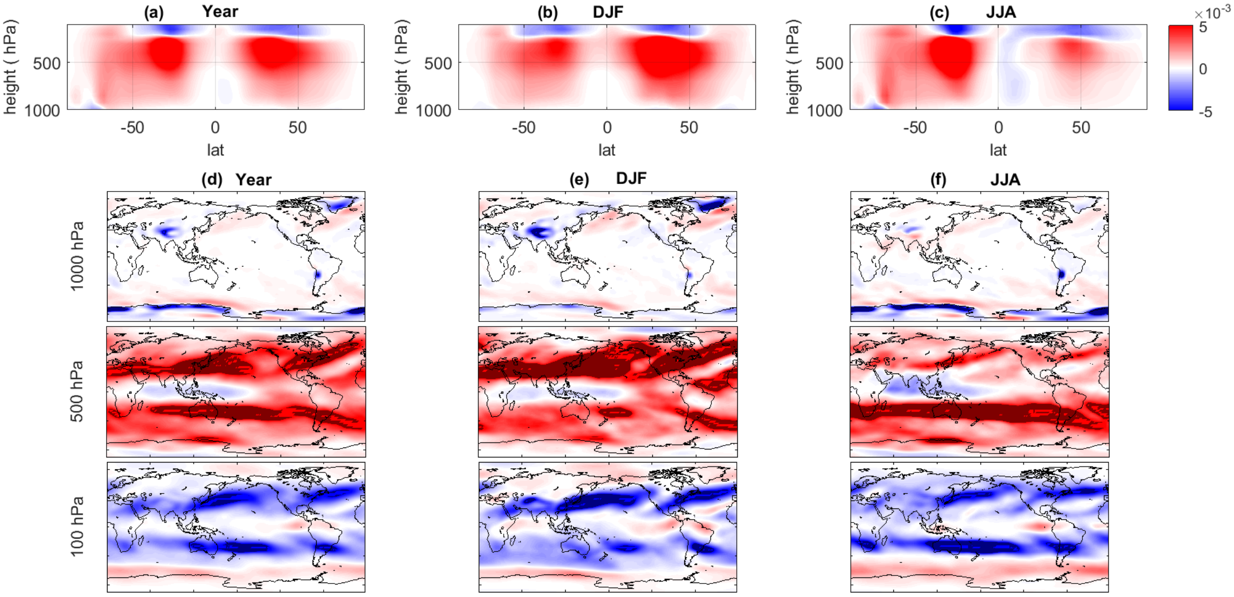

FIG. 2. Distribution of $\mathscr{D}_\ell(\vec{u}, b)$ for $\ell = 220$ Km and the NCAR reanalysis. (a-c) longitudinal averages, (d-e-f) maps at three different fixed height: 1000 hPa, 500 hPa and 100hPa. (a,d) yearly averages, (b,e) winter averages, (c,f) summer averages.

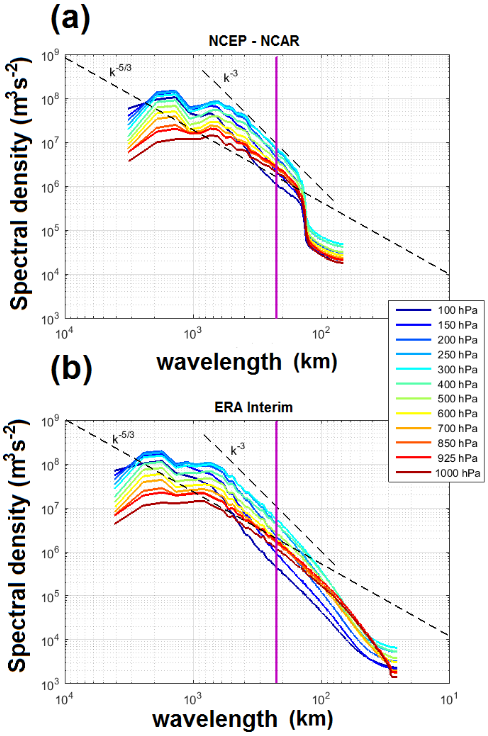

FIG. 3. Solid lines: spectra $E(k)$, where k is the wavelength) computed, at each pressure level, for the horizontal velocity fields. Dotted lines: -5/3 and -3 slopes. Magenta vertical lines: $\ell = 220$ Km. (a): NCEP-NCAR reanalysis, (b): ERA Interim reanalysis.

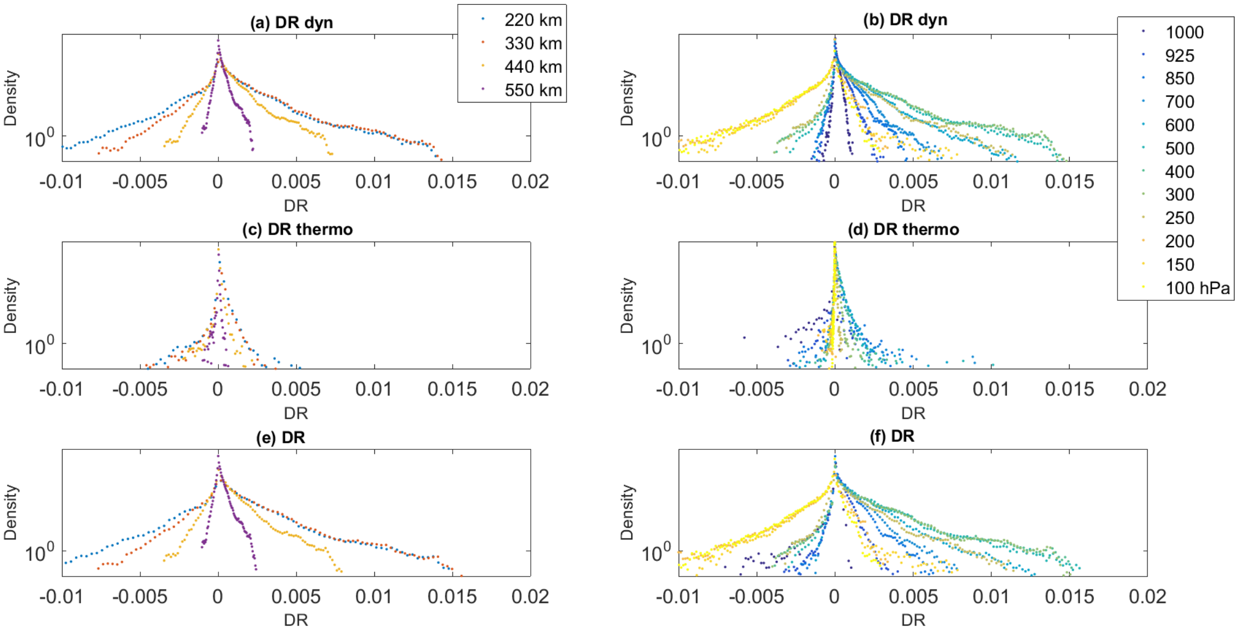

FIG. 4. Empirical $\mathscr{D}_\ell(\vec{u},b)$ density functions for ERA-Interim against scale ℓ of analysis (a,c,e) or height for $\ell = 220$ km (b,d,f). (a,b) panels show the dynamical $\mathscr{D}_\ell(\vec{u})$ component, (c,d) the thermodynamic $\mathscr{D}_\ell^T$ component and (e,f) the total $\mathscr{D}_\ell(\vec{u})$.

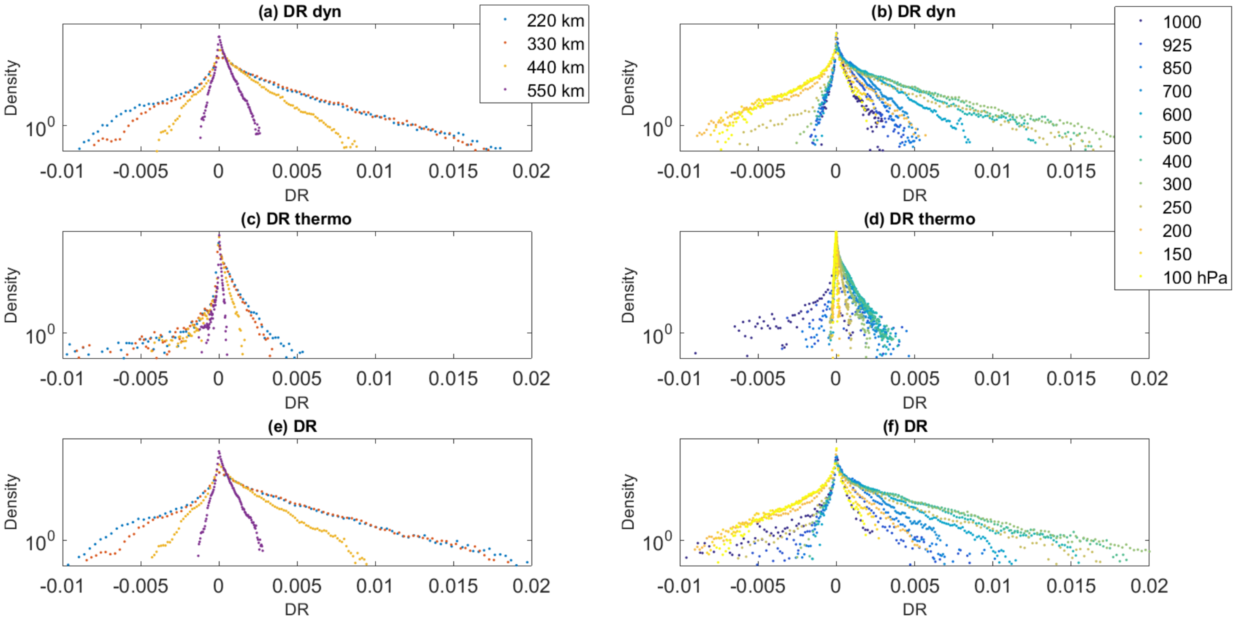

FIG. 5. Empirical $\mathscr{D}_\ell(\vec{u})$ density functions for NCAR reanalysis against scale ℓ of analysis (a,c,e) or height for $\ell = 220$ km (b,d,f). (a,b) panels show the dynamical $\mathscr{D}_\ell(\vec{u})$ component, (c,d) the thermodynamic $\mathscr{D}_\ell^T$ component and (e,f) the total $\mathscr{D}_\ell(\vec{u})$.